



Effective hydraulic properties of 3D virtual stony soils identified by inverse modeling

Mahyar Naseri*, Sascha C. Iden, and Wolfgang Durner

Division of Soil Science and Soil Physics, Institute of Geoecology, Technische Universität Braunschweig, Germany

*Corresponding author: m.naseri@tu-bs.de, Langer Kamp 19c, 38106 Braunschweig, Germany

s.iden@tu-bs.de, Langer Kamp 19c, 38106 Braunschweig, Germany

w.durner@tu-bs.de, Langer Kamp 19c, 38106 Braunschweig, Germany

Core Ideas

- Virtual stony soils with different rock fragment contents were generated in 3D using the Hydrus 2D/3D software.
- Evaporation experiments and unit-gradient experiments were numerically simulated.
- We used inverse modelling with the Richards equation to identify effective hydraulic properties of virtual stony soils.
- The identified hydraulic properties were used to evaluate the scaling models of calculating hydraulic properties of stony soils.

Keywords

Soil hydraulic properties, water retention curve, hydraulic conductivity, stony soil, inverse modeling, Hydrus 2D/3D

Abstract

Stony soils that have a considerable amount of rock fragments are widespread around the world. However, experiments to determine effective hydraulic properties of stony soils (SHP), i.e. the water retention curve (WRC) and hydraulic conductivity curve (HCC), are challenging. Installation of measurement devices and sensors in these soils is difficult and the data are less reliable because of high local heterogeneity. Therefore, effective properties of stony soils especially in unsaturated hydraulic conditions are still not well understood. An alternative approach to evaluate



the SHP of these systems with internal structural heterogeneity is numerical simulation. We used the Hydrus 2D/3D software to create virtual stony soils in 3D and simulate water flow for different volumetric rock fragment contents, *f*. Soils with volumetric stone contents from 11 to 37 % were created by placing impermeable spheres in the form of rock fragments in a sandy loam soil. Time series of local pressure heads in various depths, mean water contents and fluxes across the upper boundary were generated in a virtual evaporation experiment. Additionally, a multi-step unit gradient simulation was applied to determine effective values of hydraulic conductivity near saturation up to $pF=2$. The generated data were evaluated by inverse modeling, assuming a homogeneous system, and the effective hydraulic properties were identified. The effective properties were compared with predictions from available scaling models of SHP for different volumes of rock fragments. Our results showed that scaling the WRC of the background soil based on only the value of *f* gives acceptable results in the case of impermeable rock fragments. However, the reduction of conductivity could not be simply scaled by the value of *f*. Predictions were highly improved by applying the Novák, Maxwell, and GEM models to scale the HCC. The Maxwell model matched the numerically identified HCC best.

1. Introduction

Stony soils are soils with a considerable amount of rock fragments and are widespread in mountainous and forested watersheds around the world (Ballabio et al., 2016; Novák and Hlaváčiková, 2019). Rock fragments in soil are particles with an effective diameter of larger than 2 mm (Tetegan et al., 2015; Zhang et al., 2016). Their existence in soil influences the two constitutive soil water relationships known as soil hydraulic properties (SHP) i.e. water retention curve (WRC), and hydraulic conductivity curve (HCC) (Russo, 1988; Durner and Flühler, 2006). The accurate identification of SHP is a prerequisite for adequate prediction of water flow in soil with the Richards equation (Farthing and Ogden, 2017; Haghverdi et al., 2018). The SHP depend on soil texture and structure (Kutilek, 2004; Lehmann et al., 2020), and are influenced by the presence of rock fragments in soil. It is generally accepted that rock fragments decrease the water storage capacity of soils and its effective unsaturated hydraulic conductivity. In contrast, the formation of macropores in the vicinity of embedded rock fragments may lead to an increase in saturated hydraulic conductivity. While experimental evidence and theoretical analyses show that the volumetric content of rock fragments, *f* ($m^3 m^{-3}$), has the highest influence on effective SHP of stony soil, the effect of other characteristics of rock fragments such as their porosity, shape, size, arrangement, and orientation towards flow is less clear (Hlaváčiková and Novák, 2014; Hlaváčiková et al., 2016; Naseri et al., 2020). Up to the present, two approaches have been dominant in identifying the hydraulic behavior of stony soils: I) Experimental setups with the aim of measuring SHP of stony



soils in the field or in controlled systems in the laboratory (Cousin et al., 2003; Dann et al., 2009; Grath et al., 2015; Beckers et al., 2016; Naseri et al., 2019), and II) Development of empirical, physical or physico-empirical approaches to scale hydraulic properties of background soil based on the volumetric content of rock fragments (f) and their characteristics (Novák et al., 2011; Naseri et al., 2020). These two approaches have some systematic limitations that restrict their applications in investigating the hydraulic behavior of stony soils. Installation of sensors and measurement instruments in the stony soils are technically demanding (Cousin et al., 2003; Verbist et al., 2013; Coppola et al., 2013; Stevenson et al., 2021), undisturbed sampling is laborious (Ponder and Alley, 1997), relatively larger samples are required (Germer and Braun, 2015), and the measured data might be more inconsistent due to the higher local heterogeneity of such soils (Baetens et al., 2009; Corwin and Lesch, 2005). Furthermore, some of the available scaling models to obtain effective SHP are conceptually oversimplified and they exclusively consider the volume of rock fragments as the only input parameter (Bouwer and Rice, 1984; Ravina and Magier, 1984). Additionally, they assume impermeable rock fragments and are proposed mainly for saturated flow conditions. These scaling models need a systematic verification under variably-saturated conditions using experimental data or 3D simulations. Some reviews of these models and their evaluation are available in the literature (Brakensiek et al., 1986; Novák et al., 2011; Beckers et al., 2016; Naseri et al., 2019).

Hlaváčiková and Novák (2014) proposed a model to scale the HCC of the background soil, parametrized with the van Genuchten–Mualem (van Genuchten, 1980) model, using the model of Bower and Rice (1984). Hlaváčiková et al., (2018) used the water content of rock fragments as input parameter to scale the WRC of the background soil. Naseri et al. (2019) used the simplified evaporation method (Peters et al., 2015) to experimentally determine the effective SHP of small soil samples containing various amounts of rock fragments. Their study criticizes the application of the scaling models developed for saturated stony soils to unsaturated conditions and emphasizes the need to develop approaches that consider more characteristics of the rock fragments to calculate SHP of the stony soils.

Recent advancements in computational hydrology and computing power suggest the numerical simulation of soil water dynamics as a promising alternative to the measurement of effective SHP of heterogeneous soils (Durner et al., 2008; Lai and Ren, 2016; Radcliffe and Šimůnek, 2018). Numerical simulations have several advantages. They do not demand strict experimental setups, are repeatable under a variety of initial and boundary conditions, and in contrast to the laboratory experiments, space and time scales are not restrictive factors in the simulations. These assets have



made them a favorable tool in water and solute transport modeling in heterogeneous soils (Abbasi et al., 2003; Šimůnek et al., 2016). However, with few exceptions, heterogeneous soils like stony soils have been simulated only for simplified cases, i.e., either under fully saturated conditions or with reduced dimensionality, i.e., simulations of stony soils in two spatial dimensions (2D). Novák et al. (2011) calculated effective saturated hydraulic conductivity (K_s) of soils containing impermeable rock fragments using steady-state simulations with the software Hydrus 2D which solves the Richards equation in two spatial dimensions. They derived a linear relationship between the K_s of stony soil and f . Hlaváčiková et al. (2016) simulated different shapes and orientations of rock fragments in Hydrus 2D to obtain the effective K_s of the virtual stony soils. Beckers et al. (2016) used Hydrus 2D simulations to extend the investigations towards the impact of different volumetric rock fragment contents, shape, and size on the HCC. They also identified effective SHP of a silt loam soil containing rock fragments using laboratory evaporation experiments for rock fragment contents up to 20 % (v/v).

The inverse modeling approach has been applied to identify effective hydraulic properties of soils in laboratory experiments (Ciollaro and Romano, 1995; Hopmans et al., 2002; Nasta et al., 2011), in lysimeters and field (Abbaspour et al., 1999; Abbaspour et al., 2000), virtual lysimeters with internal textural heterogeneity (Durner et al., 2008; Schelle et al., 2013), and WRC of stony soils through field infiltration experiments (Baetens et al., 2009). Although theoretical studies and laboratory investigations on packed samples are insufficient to understand fully the hydraulic processes in stony soils, they do lead the way to the improvement and validation of effective models and their application at the field and even larger scales. Inverse modeling is arguably the best approach to achieve these aims because it allows to validate effective models using process modeling. Our aim in this study was to investigate the application of inverse modeling to identify the effective SHP of 3D virtual stony soils and to explore its applicability to these soil systems as an example of internal structural heterogeneity. We were interested in answering the following questions:

i) Is it possible to describe the dynamics in the heterogeneous 3D system with the 1D Richards equation assuming a homogeneous soil?

ii) If so, what are the effective SHP of stony soils and how are they related to the SHP of the background soil?

To answer these questions we conducted forward simulations of water movement in 3D using the Richards equation as variably-saturated flow model. We created stony soils by embedding voids representing impermeable spherical rock fragments as inclusions into a homogeneous background soil. Then we simulated transient evaporation



109 experiments and stepwise steady-state, unit-gradient infiltration experiments in 3D. The generated data were used as
 110 an input to a 1D inverse model to obtain the effective SHP of stony soils, and these properties were used to evaluate
 111 and compare the available scaling models of SHP for stony soils.

112 2. Materials and methods

113 2.1. Simulation model

114 The Hydrus 2D/3D software was used to generate virtual stony soils and simulate the water flow in the created three-
 115 dimensional geometries. Water flow in Hydrus 2D/3D is modelled by the Richards equation (Šimůnek et al., 2006;
 116 2008), which is the standard model for variably-saturated water flow in porous media. The Hydrus 2D/3D software
 117 solves the mixed form of the Richards equation numerically using the finite-element method and an implicit scheme
 118 in time (Celia et al., 1990; Šimůnek et al., 2008; 2016; Radcliffe and Šimůnek, 2018). The three-dimensional form of
 119 the Richards equation under isothermal conditions, without sinks/sources, and assuming an isotropic hydraulic
 120 conductivity is:

$$\frac{\partial \theta}{\partial t} = \frac{\partial}{\partial x} \left[K(h) \left(\frac{\partial h}{\partial x} \right) \right] + \frac{\partial}{\partial y} \left[K(h) \left(\frac{\partial h}{\partial y} \right) \right] + \frac{\partial}{\partial z} \left[K(h) \left(\frac{\partial h}{\partial z} + 1 \right) \right] \quad (1)$$

121 where θ is the volumetric water content ($\text{cm}^3 \text{cm}^{-3}$), t is time (s), h is the pressure head (cm), and $K(h)$ is the hydraulic
 122 conductivity function (cm d^{-1}). x , and y (cm) are the horizontal Cartesian coordinates, and z (cm) is the vertical
 123 coordinate, positive upwards. We used the van Genuchten-Mualem model to parametrize the WRC and HCC (van
 124 Genuchten, 1980):

$$S_e(h) = \frac{\theta(h) - \theta_r}{\theta_s - \theta_r} = [1 + (\alpha h)^n]^{-m} \quad (2)$$

125 and

$$K(h) = K_s S_e^r \left[1 - \left(1 - S_e^{\frac{1}{m}} \right)^m \right]^2 \quad (3)$$



126 where θ_s and θ_r are the saturated and residual water contents ($\text{cm}^3 \text{cm}^{-3}$), respectively, $S_e(h)$ is the effective saturation
 127 $(-)$, α (cm^{-1}) is a shape parameter, n is an empirical parameter related to the pore size distribution $(-)$ and $m = 1 -$
 128 $1/n$, K_s is the saturated hydraulic conductivity and τ is a tortuosity/connectivity parameter $(-)$.

129 2.2. 3D geometries representing stony soils

130 The virtual stony soils in 3D were created by placing spherical inclusions in a background soil. In accordance with
 131 real laboratory experiments (not reported here), we generated virtual soil columns as cylinders with a diameter of 16
 132 cm and a height of 10 cm and an total volume of $\approx 2011 \text{ cm}^3$. The inclusions were considered as voids representing
 133 impermeable rock fragments embedded in the background soil. Configurations and characteristics of the created 3D
 134 geometries of stony soils are illustrated in Fig. 1. Each spherical inclusion had a diameter of 3.04 cm and a volume of
 135 $\approx 14.7 \text{ cm}^3$. Stony soils with different volumetric rock fragment contents were created by including different numbers
 136 of spherical inclusions in the soil column. A total number of 15, 27, 39, and 51 spherical inclusions in each column
 137 led to four volumetric rock fragment contents of 11.0, 19.8, 28.5 and 37.3 % (v/v). Spheres were arranged in the
 138 column in three layers. The spheres' centers were in depths of 2.5, 5.0 and 7.5 in the column and each layer was
 139 packed with one-third of the total number of intended spheres. Furthermore, observation points at selected nodes of
 140 the numerical grid were inserted in each of the three depths of the column (i.e. 2.5, 5.0 and 7.5 cm) in the background
 141 soil and not in close vicinity of the inclusions to provide time series of soil water pressure head for the inverse
 142 simulations. For the background soil, a homogenous sandy loam soil was considered with the van Genuchten-Mualem
 143 model parameters $\theta_s = 0.410$ ($\text{cm}^3 \text{cm}^{-3}$), $\theta_r = 0.065$ ($\text{cm}^3 \text{cm}^{-3}$), $\alpha = 0.01$ (cm^{-1}), $n = 2.0$ $(-)$, $\tau = 0.5$ $(-)$, and $K_s =$
 144 100 (cm d^{-1}). The targeted mesh size for the different simulations was set to 0.25 cm. The dependency of the numerical
 145 solution on the mesh size was tested with some refined meshes and negligible differences in the results were obtained
 146 for different mesh sizes.

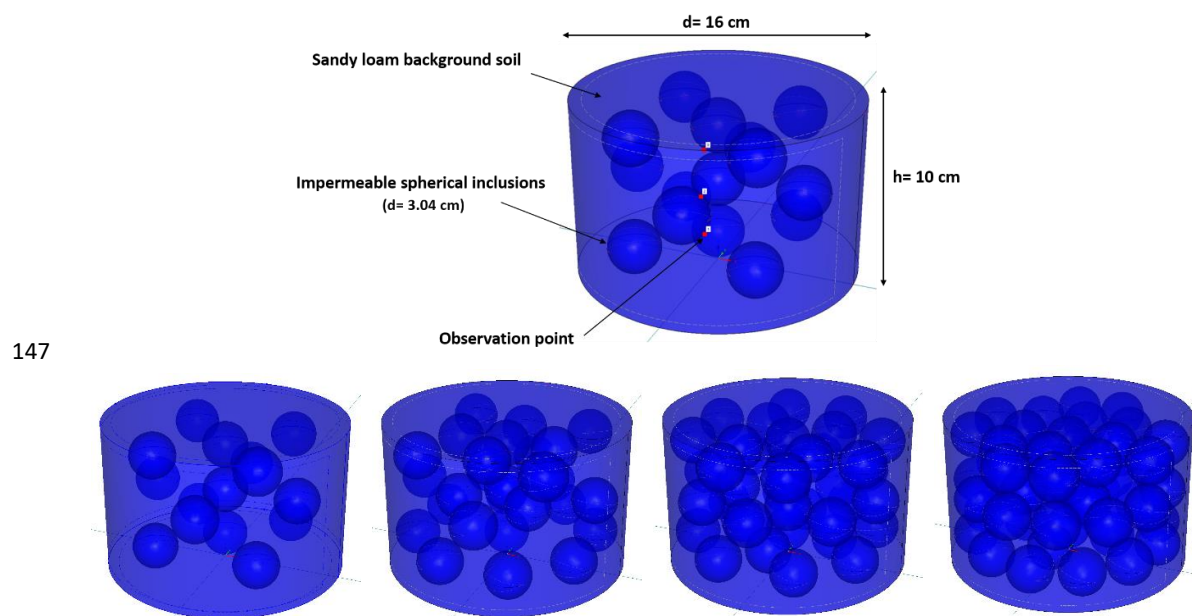


Figure 1: Visualization of 3D configurations of the generated stony soils including the dimension of rock fragments and soil cylinder and location of the observation points (top). Bottom row shows rock fragment contents of 11.0, 19.8, 28.5 and 37.3 %, from left to right.

2.3. Forward simulations

We simulated evaporation (EVA) (Peters and Durner, 2008) and multistep unit gradient (MSUG) experiments (Sarkar et al., 2019). For EVA, a linear distribution of pressure head (-2.5 cm top, +7.5 cm bottom) was used as the initial condition. The boundary conditions were no-flux at the bottom and atmospheric with a constant potential evaporation rate of 0.6 (cm d⁻¹) and zero precipitation at the top. The EVA experiments were simulated for 10 days and the time series of pressure heads at each observation point, the initial volumetric water content and the cumulative evaporation and evaporation rate were collected for later use in the inverse simulations.

In the MSUG experiment, the soil column was initially fully saturated with a constant pressure head of 0 cm. A sequence of step-wise decreasing constant pressure heads was assigned to the upper and lower boundaries of the column. The duration of the MSUG was 100 days and the pressure head in the upper and lower boundaries was simultaneously decreased stepwise to a pressure head of -100 cm. The applied pressure heads h_i were 0, -1, -3, -10, -20, -30, -60, and -100 cm, respectively. Time steps were chosen such that a steady-state flow condition was reached



for each pressure step, indicated by identical water fluxes at the top (inflow) and bottom (outflow) boundaries and constant pressure heads at the observation points. The hydraulic conductivities at the respective pressure heads h_i data were calculated by dividing the steady-state water flux rates ($\text{cm}^3 \text{ d}^{-1}$) by the total surficial area of the soil column ($\approx 202 \text{ cm}^2$).

The converging and diverging flow field around obstacles produces even under unit gradient conditions spatially different pressure heads, and as opposed to saturated conditions, these different pressure heads are under unsaturated conditions associated with different water saturations and different local hydraulic conductivities. We were interested in whether and to what extent this could lead to nonlinear effects in the derivation of the effective hydraulic properties, in particular the effective HCC. Furthermore, since the flow field for a given volume fraction of obstacles depends on dimensionality, i.e., is different in a 2D simulation than in a 3D simulation, studying the effects in the unsaturated region was one of the main motivations for performing this numerical analysis in 3D.

2.4. Inverse modeling of evaporation in 1D

A 10-day evaporation experiment in 1D was simulated with the software package HYDRUS-1D (Šimůnek et al., 2006; 2008) to obtain the SHP parameters using inverse modeling. The generated data from the EVA and MSUG forward simulations in 3D were used as an input to the 1D inverse simulations. Time series of the pressure heads at three observation depths, mean volumetric water contents in the column during the EVA experiment, and the data points of the effective HCC from the MSUG experiment were used as data in the objective function. The time series of the mean volumetric water content was calculated from the initial water content, cumulative evaporation and soil volume. The measurement range for pressure heads used in the objective function was from saturation down to -2000 cm . This reflects a setup with laboratory tensiometers with boiling delay (Schindler et al., 2010). The time series of the simulated evaporation rates from the 3D simulations were used as the time variable atmospheric boundary condition for the 1D inverse simulations. The 1D soil profile was 10 cm long and was discretized into 100 equally sized finite elements. Similar to the 3D simulations, three observation points were defined in the depths of 2.5 , 5.0 and 7.5 cm . A no-flux boundary condition was used at the bottom. The six parameters of the van Genuchten model occurring in Eq. (2) and (3) were all simultaneously estimated by inverse modeling. The weighted-least-squares objective function was minimized by the SCE-UA algorithm (Duan et al., 1992). The data obtained from the EVA experiment allows to identify the WRC from saturation to the pressure where the tensiometers fail, and the HCC in the mid to dry range of



the SHP (roughly -100 to -2000 cm pressure head), while the MSUG provides a precise determination of the HCC in the wet range (Sarkar et al., 2019; Durner and Iden, 2011). As evaporation experiments do not provide information on hydraulic conductivity near water-saturation (Peters et al., 2015), we included the MSUG data in the object function for the inverse simulation of the EVA experiments to improve the uniqueness of the inverse solution and the precision of the identified HCC near saturation (see Schelle et al., 2010, for another example).

2.5. Predicting SHP of stony soils by scaling models

The SHP of stony soils obtained by inverse modeling were compared to SHP that are predicted by available scaling models and used for their evaluation. Considering that the volumetric content of rock fragments has the dominant influence on the WRC of a stony soil, a common approach is partitioning the WRC and HCC of stony soil based on the volume of each component in the soil-rock mixture and calculating the effective SHP of stony soil using the volume averaging or the composite-porosity model. The general form of the WRC model considers the moisture contents of the background soil $\theta_{\text{soil}}(h)$ ($\text{cm}^3 \text{ cm}^{-3}$) and embedded rock fragments $\theta_{\text{rock}}(h)$ ($\text{cm}^3 \text{ cm}^{-3}$) to calculate the effective WRC of stony soils $\theta_m(h)$ ($\text{cm}^3 \text{ cm}^{-3}$) (Flint and Childs, 1984; Peters and Klavetter, 1988) with the following form in the full moisture range (Naseri et al., 2019):

$$\theta_m(h) = f\theta_{\text{rock}} + (1 - f)\theta_{\text{soil}} \quad (4)$$

A typical assumption in stony soils hydrology is that the porosity of rock fragments is negligible. In this case, Eq. (4) reduces to (Bouwer and Rice, 1984):

$$\theta_m(h) = (1 - f)\theta_{\text{soil}} \quad (5)$$

For the effective hydraulic conductivity of stony soils, some scaling models are developed for saturated conditions that might apply to the hydraulic conductivity at any pressure heads. The simplest scaling model accounts only for the reduction in the cross-sectional area available for flow of water. This leads to the equation (Ravina and Magier, 1984):

$$K_r = 1 - f \quad (6)$$

where $K_r(-)$ is the relative hydraulic conductivity of stony soil, i.e., $K_r = K_m/K_{\text{soil}}$, where K_m is the effective hydraulic conductivity of the stony soil (cm d^{-1}), and K_{soil} is the conductivity of the background soil (cm d^{-1}).



In a more recent approach, Novák et al. (2011) developed a linear relationship based on the 2D numerical simulation results as a first approximation to scale the saturated hydraulic conductivity of stony soils:

$$K_r = 1 - \alpha f \quad (7)$$

The parameter α was reported to depend on the texture of the background soil, with a range between 1.1 for sandy clay to 1.32 for clay. This model is easy to apply, but it requires the estimation of the parameter α to calculate K_r . For our calculations, we assumed $\alpha = 1.2$ for the sandy loam background soil used in our study.

Another model that has been developed for mixtures with spherical inclusions is the Maxwell model (Maxwell, 1873; Corring and Churchill, 1961; Peck and Watson, 1979; Zimmermann and Bodvarsson, 1995). It takes the volumetric rock fragment content, hydraulic conductivity of the background soil and hydraulic conductivity of inclusions into account to calculate the hydraulic conductivity of the stony soil. In the special case of impermeable inclusions, Maxwell model reduces to:

$$K_r = \frac{2(1-f)}{2+f} \quad (8)$$

A recently developed model by Naseri et al. (2020), which is based on the general effective medium theory (GEM), allows considering effects of permeability, shape, and orientation of rock fragments on the effective HCC. For impermeable rock fragments, the GEM model reduces to the following form:

$$K_r = \left(1 - \frac{f}{f_c}\right)^t \quad (9)$$

where f_c is the critical rock fragment content with values between 0.84 and nearly 1 and t is a shape parameter with values between 1.26 and nearly 1.5 for spherical rock fragments. In this study, we set the critical rock fragment to $f_c = 0.982$ (v/v) according to the size ratio of the rock fragments to the background soil, and $t = 1.473$ for spherical rock fragments (for details, see appendix in Naseri et al., 2020).

It should be noted that all approaches apply at any pressure head h_i , i.e., the scaling that is originally developed for saturated conditions with locally constant hydraulic conductivity in the background soil is equally applied to unsaturated conditions.



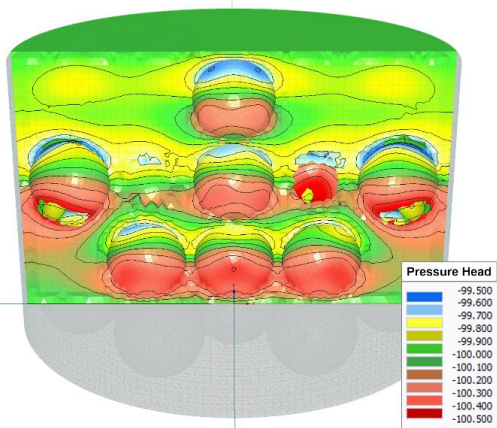
231 3. Results and discussion

232 3.1. Flow field and variability of state variables in the MSUG experiment

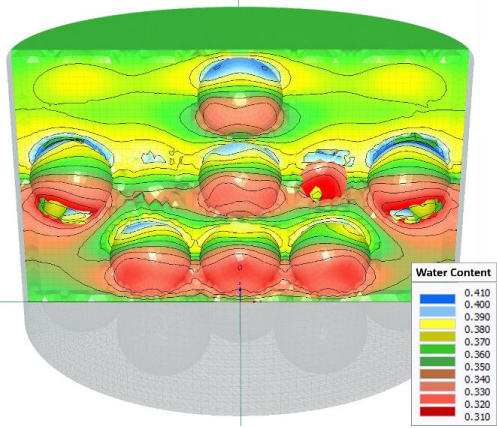
233 Figure 2 visualizes the pressure head (cm), water content ($\text{cm}^3 \text{cm}^{-3}$), and velocity (cm d^{-1}) in a 2D cross section in the
234 center of the soil column through the forward simulation of the MSUG experiment. The profile is shown for the steady
235 state flux situation with a pressure head of -100 cm and the stony soil with 28.5 % rock fragment content. The Figure
236 shows a considerable change in the flow velocities, even at the upper boundary. Also, as Fig. 2 illustrates, the
237 conditions above an obstacle might be slightly wetter than below an obstacle, but the variations in the pressure head
238 and the water content fields is very small. We note that this general finding was equally applicable for all other pressure
239 heads steps in the MSUG experiment.



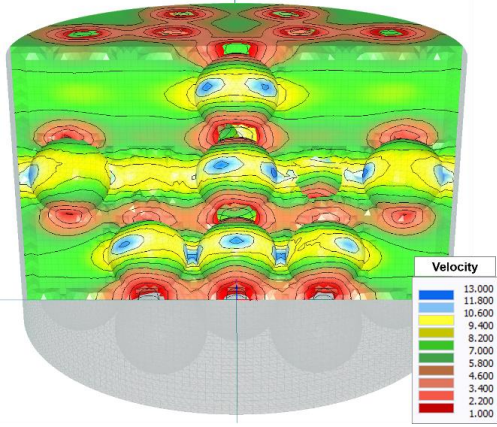
240



241



242

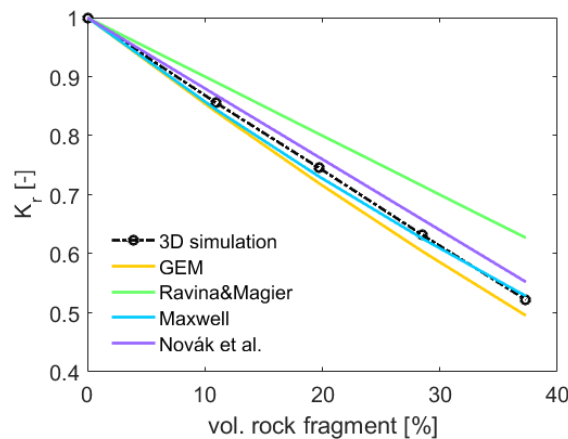


243 *Figure 2: Visualization of the pressure head (cm), water content (cm³ cm⁻³), and velocity (cm d⁻¹) in a 2D profile in the center of*
244 *the soil column during the forward simulation of MSUG experiment.*



3.2. Comparison of the relative K_r of the scaling models and the 3D simulations under saturated conditions

The dependency of the relative saturated hydraulic conductivity (K_r) on the percentage of rock fragments, calculated by different scaling models and the obtained values from the first pressure in the MSUG experiment is presented in Fig. 3. The results of the models are shown up to the $f = 37.3$ %, which was the highest value of f simulated in 3D. However, some of the evaluated models are theoretically valid for higher or lower values of f , e.g. 40 % for the Novák et al. (2011) model and higher values for the GEM model (Naseri et al., 2020).



251

252 *Figure 3: Comparison of the values of K_r (-) from the MSUG experiment in 3D (circles), and calculated by different scaling models*
 253 *(solid lines) for volumetric rock fragments up to 37.3 %. The dashed line connects the simulated data points of K_r shown by circles.*

254 Obviously, the results of our simulations confirm a linear reduction of K_r with increasing volumetric rock fragments
 255 up to $f = 37.3$ % (v/v) in the soil. The numerically obtained values of K_r are shown by circles and connected by the
 256 dashed line in Fig. 3. The dashed line has a slope of -1.29 representing a higher reduction rate of K_r compared to the
 257 scaling of K_r that would be proportional to the volumetric rock fragment content, expressed by Eq. (6) and predicted
 258 by the model of Ravina and Magier (1984) (solid green line). This result supports the fact that even in a stony soil
 259 with spherical impermeable rock fragments, the reduction in the hydraulic conductivity is higher than the reduction
 260 of the average cross-sectional area (which is statistically equivalent to the volumetric fraction of rock fragments).
 261 Hlaváčiková et al. (2016) found an even higher value of -1.45 for spherical rock fragments with a diameter of 10 cm.
 262 The model of Novák et al. (2011) performs better but also leads to a slight under-prediction of the reduction of the



263 effective saturated conductivity. The performance of this model could be improved by adjusting the parameter α to
264 match the data of the 3D simulation, but doing this would lead to an unfair comparison with the other models.

265 The two models predicting a nonlinear relationship between the K_r and f , GEM and Maxwell, show similar results at
266 low contents of rock fragments up to 10 %, with minor differences in outputs of the models. Among all of the evaluated
267 models of scaling K_s , the Maxwell model yields the closest match to the numerically identified values of K_r .

268 We note that these results may differ in natural soils, where an increase of the saturated hydraulic conductivity might
269 be expected because of macropore flow in lacunar pores at the interface between background soil and rock fragments
270 (Beckers et al., 2016; Hlaváčiková et al., 2019, Arias et al., 2019). We have not included such a process in our 3D
271 simulations.

272 3.3. Inverse modeling results for effective hydraulic properties

273 The observed and fitted time series of the pressure heads at the three representative observation points is shown in
274 Fig. 4 for the simulated experiments of the four cases with different volumetric rock fragment contents. In each case,
275 the fitted pressure heads at the three depths of the column (2.5, 5.0 and 7.5 cm) match well with the time series of the
276 corresponding data from the 3D virtual experiments. Specifically, the match of the pressure heads at 7.5 and 5.0 cm
277 is excellent, whereas there are slight systematic deviations at the uppermost level at the later stage of the evaporation
278 experiment.

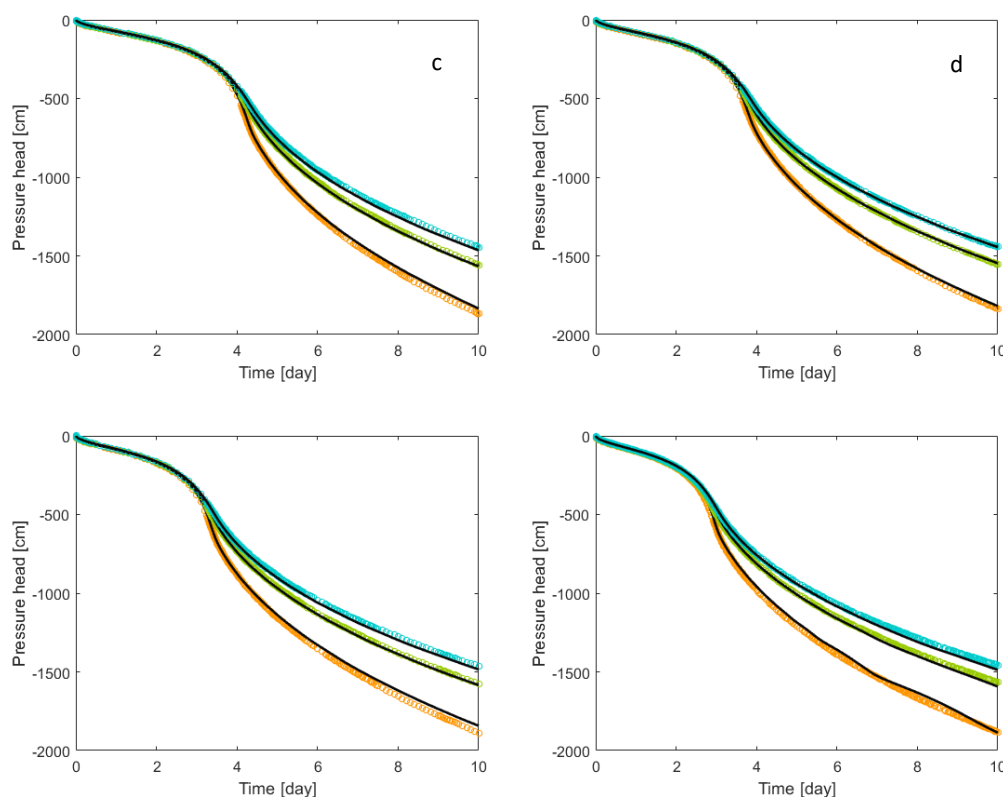


Figure 4: The time series of the 3D-simulated (circles) and 1D-fitted (solid lines) pressure heads at the observation points in three depths of the stony soil columns with a) 11.0 %, b) 19.8 %, c) 28.5 %, and d) 37.3 % volumetric rock fragment contents (v/v). The observation depths are indicated by different color codes of orange (upper, 2.5 cm), green (middle, 5.0 cm) and blue (lower, 7.5 cm from top).

Table 1 shows the values of the root mean square error (RMSE) and mean absolute error (MAE) between the observed and fitted time series of the pressure heads at three observations points for different contents of rock fragments. According to the Table 1, the fit is best for the lower rock fragment and in the middle of the column. The highest deviations occur for the highest rock fragment content but there is no clear trend. Overall, the values of RMSE and MAE are in an acceptable range regarding the observed values of pressure heads up to -2000 cm. This indicates that the time series of the pressure heads at multiple depths generated by the 3D simulations of evaporation experiments can be described successfully by the 1D Richards equation assuming a homogenous system with effective SHP.



Table 1: The values of RMSE and MAE between the observed and fitted pressure heads, in three observation points for different rock fragment contents.

Criteria	Observation point	Volumetric rock fragments (%)			
		11.0	19.8	28.5	37.3
RMSE	upper	12.8	6.5	12.6	18.9
	middle	4.9	2.8	5.3	10.7
	lower	9.1	3.1	8.7	13.9
MAE	upper	10.0	4.9	9.4	14.5
	middle	4.0	2.1	4.5	8.5
	lower	7.0	2.6	6.8	11.0

The identified SHP are presented in Fig. 5. The solid lines in the Figure show the WRC and HCC of the virtual stony soils obtained by inverse simulation (except the solid black lines, which are the WRC and HCC of the background soil), the dashed lines represent the scaled WRC by Eq. (5) and HCC by Eq. (6), and the circles on the HCC plots represent the discrete data points of hydraulic conductivity obtained by the MSUG. The WRC and HCC are presented on a pF scale, which is defined as $pF = \log_{10}(|h|)$, in which h is the pressure head in cm (Schofield, 1935). The van-Genuchten model parameters of the background soil and stony soils are shown in Table 2.

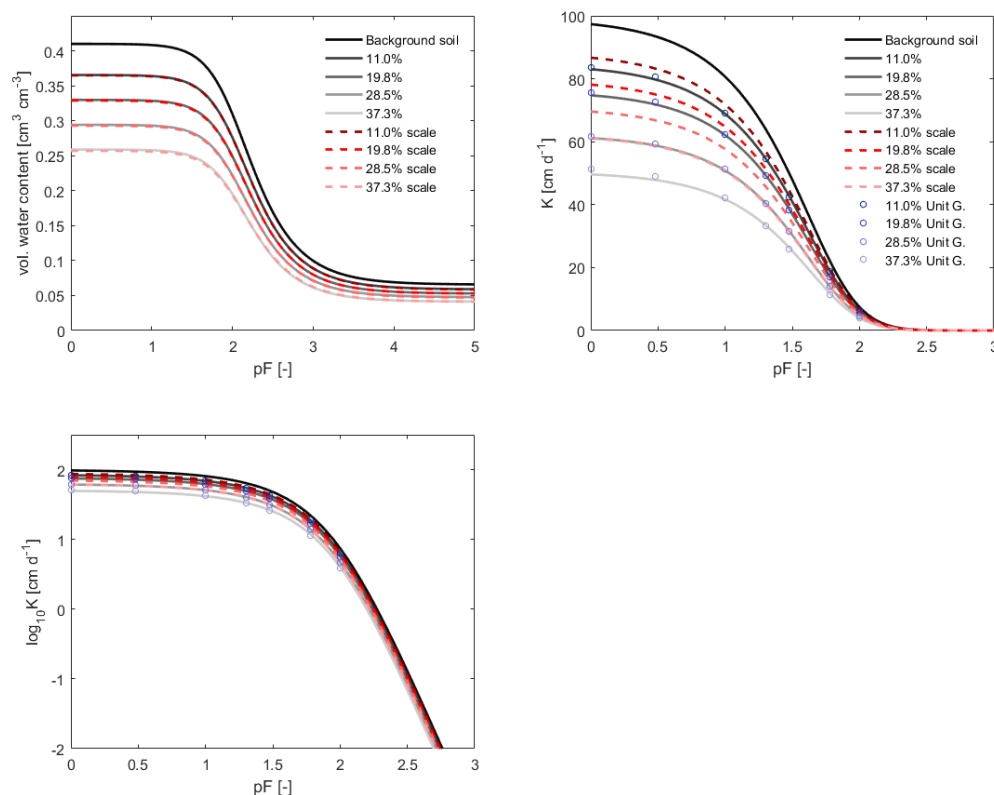


Figure 5: The WRC and HCC of the background soil (solid black line), and identified effective WRC (left) and HCC (right) of the stony soils (solid gray lines) with different volumetric rock fragments. The HCC are presented also in the logarithmic scale. The dashed lines show the effective WRC and HCC calculated by the models of Bouwer and Rice (1984) and Ravina and Magier (1984). The circles on the HCC present the data points of hydraulic conductivity obtained by the MSUG experiment in near-saturated conditions up to the $pF \approx 2$.

Table 2: The van-Genuchten model parameters of the SHP of the background soil and of the inversely determined effective SHP of the stony soils with different values of f_v .

Parameter	Unit	Volumetric rock fragments (%)				
		Background soil	11.0	19.8	28.5	37.3
θ_s	($\text{cm}^3 \text{cm}^{-3}$)	0.410	0.365	0.330	0.294	0.259
θ_r	($\text{cm}^3 \text{cm}^{-3}$)	0.065	0.059	0.053	0.048	0.041
α	(cm^{-1})	0.010	0.010	0.010	0.010	0.010
n	(-)	2.000	2.007	2.011	2.014	2.037
K_s	(cm d^{-1})	100.0	84.7	76.2	62.3	50.4
τ	(-)	0.50	0.43	0.47	0.42	0.38



314 According to the Fig. 5 and Table 2 the value of the shape parameter α is independent of the rock fragment content
 315 and the change in the value of n is negligible small (but might be systematic). The inversely identified WRC and the
 316 predictions from the Bouwer and Rice (1984) scaling model match almost perfectly for all rock fragment contents. In
 317 agreement with this, there is also an excellent agreement of the values of the saturated (θ_s) and residual water contents
 318 (θ_r) (v/v) between scaled and identified WRC. The values of θ_s and θ_r in the WRC are directly related to the
 319 volumetric rock fragment contents and the respective values of the background soil and the WRC is scaled by this
 320 factor over the whole range of soil water pressure head.

321 Similar to the WRC, an increase of the volumetric rock fragments reduces the hydraulic conductivity over the whole
 322 range of pressure head covered by the virtual experiments. However, in contrast to the WRC, the simple scaling model
 323 based on Eq. (6) cannot describe the reduction in HCC. Figure 5 shows that the model of Ravina and Magier (1984,
 324 dashed lines) underestimates the reduction of the effective HCC for all rock contents. The reason might be related to
 325 the local variations of the flow velocity in the soil column. It was shown in Fig. 2 that the variations in the water flow
 326 velocity might be considerable. The nonlinearities in the flow field and changes in the local conductivities, together
 327 with an increased average flow path length, force a stronger overall conductivity reduction. The arrangement of rock
 328 fragments thus might affect the reduction in hydraulic conductivities, leading to different conductivities at the same
 329 volumetric rock fragments (Naseri et al., 2020). The degree depends on how the flow area is altered in the soil column
 330 due to the presence of rock fragments (Fig. 1 and 2). This result is in agreement with Novák et al. (2011) who reported
 331 a higher reduction in conductivity compared to a reduction that is proportional to the rock fragments content.
 332 Furthermore, it may also differ alter depending on the characteristics of rock fragments such as their size, shape and
 333 orientation towards flow (Novák et al., 2011).

334 We had to include the data points of hydraulic conductivity from the MSUG in the inverse objective function to get a
 335 precise identification of the HCC obtained by inverse modeling near saturation. The information content from the
 336 EVA experiment gives a unique identification only when the flux rate in the system reaches te magnitude of the
 337 unsaturated hydraulic conductivity, which is for many soils around pF 1.5 to to $pF = 2$ (Peters and Durner, 2008).
 338 Although there are some discrepancies visible near saturation for the case with a high value of f , the resulting values
 339 of hydraulic conductivity from the MSUG experiment and the inversely identified HCC using the EVA experiment
 340 join well around $pF = 2$ for all of the values of f . Therefore, the HCC could be described successfully from the



341 saturation up to $pF = 3$ using the inverse modeling of the evaporation experiment with added K support points from
342 the MSUG. The overall results suggest that the effective hydraulic parameters of stony soils could be obtained by the
343 corresponding real experiments and the result is robust for both, WRC and HCC, even if the uncertainty in the identified
344 HCC is higher than that of the WRC (Singh et al., 2020; 2021).

345 **3.4. Evaluation of the Novák, Maxwell and GEM models using the identified HCC**

346 As stated above, the model of Ravina and Magier (1984) which is a linear scaling approach of the hydraulic
347 conductivity (Eq. 6) underestimates the reduction of conductivity in the stony soil. We used the identified HCC as a
348 benchmark to evaluate more advanced models of scaling HCC, namely the Novák, Maxwell and GEM models (Eqs.
349 7, 8 and 9). Figure. 6 illustrates the calculated HCC of stony soils with different volumetric rock fragments using these
350 models of scaling HCC and compares them to the identified HCC by the inverse modeling.

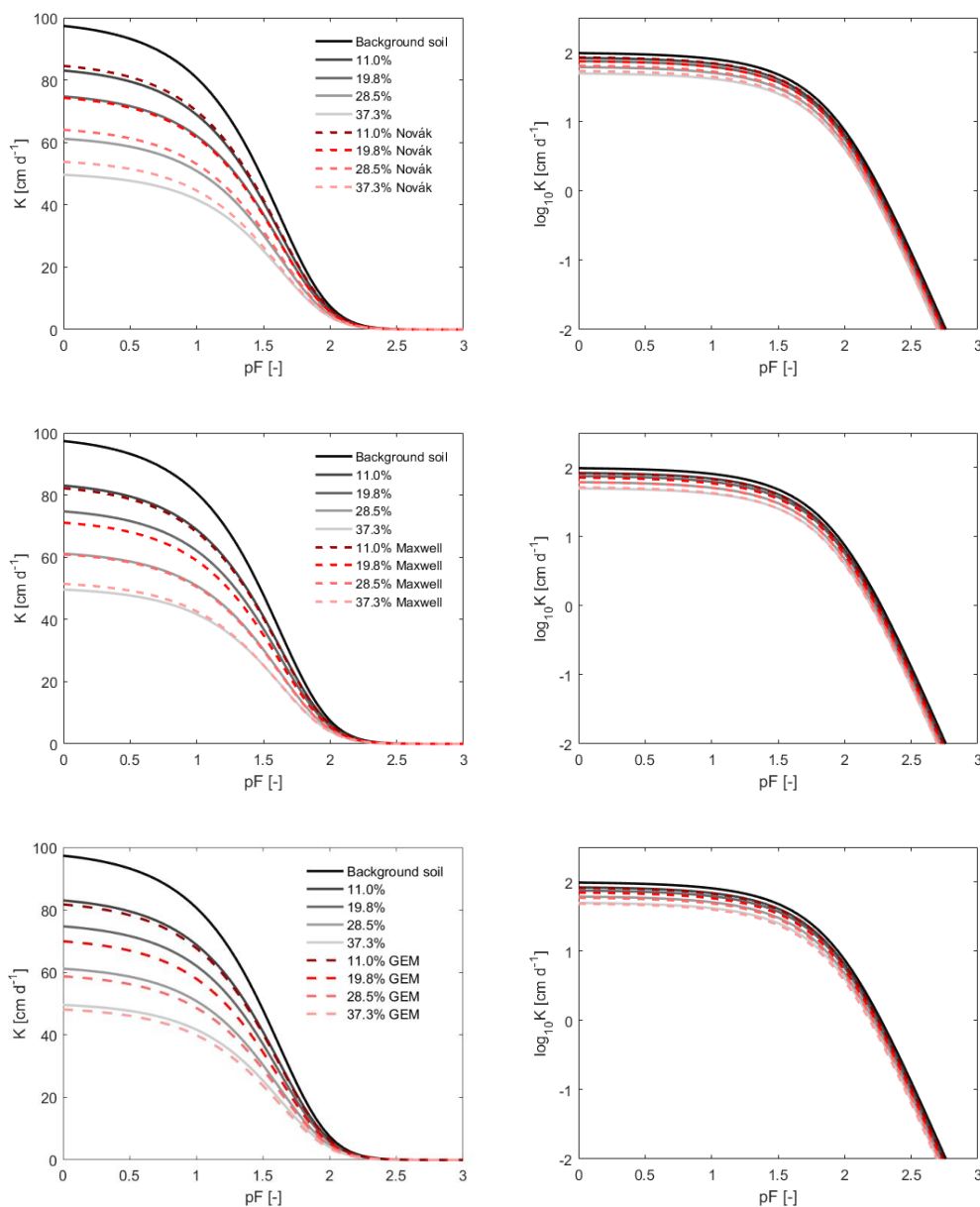


Figure 6: Evaluation of the Novák, Maxwell and GEM models of scaling HCC of stony soils using the identified HCC as a benchmark. The HCC in each case were obtained for different rock fragment contents $f=11.0, 19.8, 28.5$ and 37.3 % (v/v). The inverse identified curves are shown in solid lines and the model results in dashed lines. The value of f_c in the GEM model was set as 0.982 with the corresponding shape parameter $t=1.473$ and the parameter $\alpha = 1.2$ was selected for the Novák model.



The calculated HCC by the three models are in general in good agreement with the identified HCC in the observed range of pressure heads. All three models result in a more realistic estimate of the HCC compared to the simple linear scaling approach. While the model of Novák slightly underestimates the identified HCC for all the four rock fragment contents, the results are contrary for the GEM model where the reduction in the hydraulic conductivity is overestimated. The Maxwell model shows the same results as GEM model except for the stony soil with $f = 37.3\%$ where it underestimates the HCC.

In order to compare the performance of the three models, the average deviation (d_{avg}) between the calculated and identified HCC (logarithmic scale) was calculated to quantify the error of each model in the pF range 0 to 3 (Table 3). The signs of numbers in Table 3 represent the tendency of the model in over- or underestimating the identified hydraulic conductivities. The negative sign means the model underestimates the reduction of hydraulic conductivity.

Table 3: Performance of the Novák, Maxwell and GEM models quantified by the average deviation of $\log_{10}(K)$ (d_{avg}) for different values of rock fragments.

model	Volumetric rock fragment (%)			
	11.0	19.8	28.5	37.3
Novák	-0.0068	-0.0028	-0.0179	-0.0231
Maxwell	0.0056	0.0162	0.0039	-0.0038
GEM	0.0077	0.0234	0.0197	0.0248

371

Table 3 confirms the qualitative tendency of underestimation of the conductivity reduction by the Novák model and the overestimation by the GEM and Maxwell models, but also shows that the difference between the three models is not large and probably not of relevance in practice (the GEM model at high stone content, which has the highest deviation, corresponds to a relative mismatch of K of 6 %). However, despite the potential of the three models in predicting the HCC of stony soils, we think they require further evaluations using field measured data of hydraulic conductivity in different experimental conditions.

4. Conclusions

The objective of our study was to identify the effective SHP of stony soils by inverse modeling of flow experiments in 3D virtual soils as an alternative tool to laboratory measurements. We were interested to learn if the observed synthetic data from the forward virtual experiments in such systems with internal structural heterogeneity could be described by inverse modeling, and if so, whether unique SHP could be identified. We addressed the problem through



383 detailed 3D numerical simulations of evaporation and multistep unit gradient experiments on 3D stony soils with
 384 different amounts of impermeable spherical rock fragments. The evaporation experiments yielded synthetic data in
 385 the moisture range from saturation to pF 3, which is close to the lower limit of tensiometer measurements in real
 386 experiments. A specific focus of our analysis was on saturated/unsaturated hydraulic conductivity. We identified
 387 effective SHP by inverse simulations with the 1D Richards equation and used them to validate models of predicting
 388 HCC of stony soils. The saturated hydraulic conductivities obtained from the 3D simulations were used as a
 389 benchmark to evaluate and compare the common scaling approaches of the saturated conductivity, K_s . Secondly, the
 390 applicability of the scaling models for unsaturated conditions were investigated, namely the Bouwer and Rice (1984)
 391 model of scaling WRC, and Ravina and Magier (1984), Maxwell (Peck and Watson, 1979), Novák (Novák et al.,
 392 2011), and GEM (Naseri et al., 2020) models for scaling HCC of stony soils.

393 The boundary fluxes and the internal system states in the 3D evaporation experiments, represented by the observed
 394 time series of pressure heads at multiple depths, could be matched well by 1D simulations, and the effective WRC
 395 and HCC of the considered stony soils were determined precisely. Comparison with the scaling models showed that
 396 by assuming a homogeneous background soil and impermeable rock fragments, the effective WRC can be calculated
 397 from the WRC of fine soil using a simple correction factor equal to the volume fraction of fine soil, $(1 - f)$. That is
 398 a result with practical implications in obtaining WRC of stony soils. Also, the scaling results for HCC were promising.
 399 Our results confirmed that the reduction in K_r was stronger than calculated by a simple proportionality to $(1 - f)$.
 400 The three models of Novák, Maxwell and GEM consider this and performed adequately in calculating the HCC of the
 401 stony soils. The Maxwell model matched the numerical results best.

402 Care must be taken before generalizing these results to arbitrary conditions, e.g., highly dynamic boundary conditions
 403 with sequences of precipitation and higher and lower evaporation rates, which might result in different results due to
 404 the occurrence of non-equilibrium water dynamics and hysteresis. For real stony soils, changes in the pore size
 405 distribution of the background soil may result from the presence of rock fragments (Sekucia et al., 2020) with
 406 corresponding consequences for effective SHP. This influence is reported to be more common in compactable soils
 407 with a shrinkage-swelling potential (Fiès et al., 2002). In highly stony soils, where rock fragments are not embedded
 408 completely in the background soil, the existence of effective SHP is still an open question. Finally, the impact of



409 arrangement and size of rock fragments on evaporation dynamics and effective SHP needs to be understood. Tackling
 410 these problems requires a combination of experimental and modelling approaches.

411 References

- 412 Abbasi, F., Jacques, D., Šimůnek, J., Feyen, J. and Van Genuchten, M.T., 2003. Inverse estimation of soil hydraulic
 413 and solute transport parameters from transient field experiments: Heterogeneous soil. *Transactions of the*
 414 *ASAE*, 46(4), p.1097, doi: 10.13031/2013.13961.
- 415 Arias, N., Virto, I., Enrique, A., Bescansa, P., Walton, R. and Wendroth, O., 2019. Effect of Stoniness on the Hydraulic
 416 Properties of a Soil from an Evaporation Experiment Using the Wind and Inverse Estimation Methods. *Water*, 11(3),
 417 p.440, 10.3390/w11030440.
- 418 Ballabio, C., Panagos, P. and Monatanarella, L., 2016. Mapping topsoil physical properties at European scale using
 419 the LUCAS database. *Geoderma*, 261, pp.110-123, doi: 10.1016/j.geoderma.2015.07.006.
- 420 Beckers, E., Pichault, M., Pansak, W., Degré, A., and Garré, S., 2016. Characterization of stony soils' hydraulic
 421 conductivity using laboratory and numerical experiments. *Soil 2*: 421–431, doi: 10.5194/soil-2-421-2016.
- 422 Bouwer, H., and Rice, R.C., 1984. Hydraulic properties of stony vadose zones. *Ground Water* 22: 696–705, doi:
 423 10.1111/j.1745-6584.1984.tb01438.x.
- 424 Brakensiek, D.L., Rawls, W.J., and Stephenson, G.R., 1986. Determining the saturated conductivity of a soil
 425 containing rock fragments. *Soil Sci. Soc. Am. J.* 50: 834-835, doi: 10.2136/sssaj1986.03615995005000030053x.
- 426 Celia, M.A., Bouloutas, E.T. and Zarba, R.L., 1990. A general mass-conservative numerical solution for the
 427 unsaturated flow equation. *Water resources research*, 26(7), pp.1483-1496, doi: 10.1029/WR026i007p01483.
- 428 Coppola, A., Dragonetti, G., Comegna, A., Lamaddalena, N., Caushi, B., Haikal, M.A. and Basile, A., 2013.
 429 Measuring and modeling water content in stony soils. *Soil and Tillage Research*, 128, pp.9-22. doi:
 430 10.1016/j.still.2012.10.006.
- 431 Corwin, D.L. and Lesch, S.M., 2005. Apparent soil electrical conductivity measurements in agriculture. *Computers*
 432 *and Electronics in Agriculture*, 46(1-3), pp.11-43. doi: 10.1016/j.compag.2004.10.005.
- 433 Cousin, I., Nicoullaud, B., and Coutadeur, C., 2003. Influence of rock fragments on the water retention and water
 434 percolation in a calcareous soil. *Catena*, 53: 97–114. doi: 10.1016/S0341-8162(03)00037-7.
- 435 Dann, R., Close, M., Flintoft, M., Hector, R., Barlow, H., Thomas, S. and Francis, G., 2009. Characterization and
 436 estimation of hydraulic properties in an alluvial gravel vadose zone. *Vadose Zone Journal*, 8(3), pp.651-663, doi:
 437 10.2136/vzj2008.0174.
- 438 Durner, W. and Iden, S.C., 2011. Extended multistep outflow method for the accurate determination of soil hydraulic
 439 properties near water saturation. *Water Resources Research*, 47(8), doi: 10.1029/2011WR010632.
- 440 Durner, W., and Flühler, H., 2006. Chapter 74: Soil hydraulic properties. In M. G. Anderson, and J. J. McDonnell
 441 (Eds.), *Encyclopedia of hydrological sciences*, chapter 74 (pp. 1103–1120). John Wiley & Sons., doi:
 442 10.1002/0470848944.hsa077c.
- 443 Durner, W., Jansen, U. and Iden, S.C., 2008. Effective hydraulic properties of layered soils at the lysimeter scale
 444 determined by inverse modelling. *European Journal of Soil Science*, 59(1), pp.114-124, doi:10.1111/j.1365-
 445 2389.2007.00972.x.
- 446 Farthing, M.W. and Ogden, F.L., 2017. Numerical solution of Richards' equation: A review of advances and
 447 challenges. *Soil Science Society of America Journal*, 81(6), pp.1257-1269, doi: 10.2136/sssaj2017.02.0058.



- 448 Fiès, J.C., Louvigny, N.D.E., and Chanzy, A., 2002. The role of stones in soil water retention. *European Journal of*
 449 *Soil Science*, 53(1), pp.95-104, doi: 10.1046/j.1365-2389.2002.00431.x.
- 450 Grath, S.M., Ratej, J., Jovičić, V., and Curk, B., 2015. Hydraulic characteristics of alluvial gravels for different particle
 451 sizes and pressure heads. *Vadose Zone J.*, doi: 10.2136/vzj2014.08.0112.
- 452 Germer, K., and Braun J., 2015. Determination of anisotropic saturated hydraulic conductivity of a macroporous slope
 453 soil. *Soil Sci. Soc. Am. J.* 79: 1528-1536, doi: 10.2136/sssaj2015.02.0071.
- 454 Haghverdi, A., Öztürk, H.S. and Durner, W., 2018. Measurement and estimation of the soil water retention curve
 455 using the evaporation method and the pseudo continuous pedotransfer function. *Journal of hydrology*, 563, pp.251-
 456 259, doi:10.1016/j.jhydrol.2018.06.007.
- 457 Hlaváčiková, H., and Novák V., 2014. A relatively simple scaling method for describing the unsaturated hydraulic
 458 functions of stony soils. *J. Plant Nutr. Soil Sci.* 177: 560–565, doi: 10.1002/jpln.201300524.
- 459 Hlaváčiková, H., Novák V., and Šimůnek J., 2016. The effects of rock fragment shapes and positions on modeled
 460 hydraulic conductivities of stony soils. *Geoderma* 281: 39–48, doi: 10.1016/j.geoderma.2016.06.034.
- 461 Hlaváčiková, H., Novák, V., Kostka, Z., Danko, M. and Hlavčo, J., 2018. The influence of stony soil properties on
 462 water dynamics modeled by the HYDRUS model. *Journal of Hydrology and Hydromechanics*, 66(2), pp.181-188,
 463 doi: 10.1515/johh-2017-0052.
- 464 Hopmans J.W., Šimůnek J., Romano N., Durner W., 2002. Inverse Modeling of Transient Water Flow, In: *Methods*
 465 *of Soil Analysis, Part 1, Physical Methods*, Chapter 3.6.2, Eds. J. H. Dane and G. C. Topp, Third edition, SSSA,
 466 Madison, WI, 963–1008.
- 467 Kutilek, M., 2004. Soil hydraulic properties as related to soil structure. *Soil and Tillage Research*, 79(2), pp.175-184,
 468 doi: 10.1016/j.still.2004.07.006.
- 469 Lai, J. and Ren, L., 2016. Estimation of effective hydraulic parameters in heterogeneous soils at field scale. *Geoderma*,
 470 264, pp.28-41, doi: 10.1016/j.geoderma.2015.09.013.
- 471 Lehmann, P., Bickel, S., Wei, Z. and Or, D., 2020. Physical constraints for improved soil hydraulic parameter
 472 estimation by pedotransfer functions. *Water Resources Research*, 56(4), p.e2019WR025963, doi:
 473 10.1029/2019WR025963.
- 474 Mualem, Y., 1976. A new model for predicting the hydraulic conductivity of unsaturated porous media. *Water Resour.*
 475 *Res.* 12: 513–521, doi: 10.1029/WR012i003p00513.
- 476 Naseri, M., Iden, S. C., Richter, N., and Durner, W., 2019. Influence of stone content on soil hydraulic properties:
 477 experimental investigation and test of existing model concepts. *Vadose Zone J.*, 18:180163. doi:
 478 10.2136/vzj2018.08.0163.
- 479 Naseri, M., Peters, A., Durner, W. and Iden, S.C., 2020. Effective hydraulic conductivity of stony soils: General
 480 effective medium theory. *Advances in Water Resources*, 146, p.103765, doi: 10.1016/j.advwatres.2020.103765.
- 481 Nasta, P., Huynh, S. and Hopmans, J.W., 2011. Simplified multistep outflow method to estimate unsaturated hydraulic
 482 functions for coarse-textured soils. *Soil Science Society of America Journal*, 75(2), pp.418-425,
 483 doi:10.2136/sssaj2010.0113.
- 484 Novák, V., and Hlaváčiková, H., 2019. *Applied Soil Hydrology*. Springer International Publishing. doi: 10.1007/978-
 485 3-030-01806.
- 486 Novák, V., Křava, K., and Šimůnek, J., 2011. Determining the influence of stones on hydraulic conductivity of
 487 saturated soils using numerical method. *Geoderma*, 161: 177–181. doi: 10.1016/j.geoderma.2010.12.016.



- 488 Peters, A. and Durner, W., 2008. Simplified evaporation method for determining soil hydraulic properties. *Journal of*
489 *Hydrology*, 356(1-2), pp.147-162, doi: 10.1016/j.jhydrol.2008.04.016.
- 490 Peters, R. R., and Klavetter, E. A., 1988. A continuum model for water movement in an unsaturated fractured rock
491 mass. *Water Resources Research*, 24, 416–430.
- 492 Peters, A., Iden, S.C. and Durner, W., 2015. Revisiting the simplified evaporation method: Identification of hydraulic
493 functions considering vapor, film and corner flow. *Journal of Hydrology*, 527, pp.531-542, doi:
494 10.1016/j.jhydrol.2015.05.020.
- 495 Ponder, F. and Alley, D.E., 1997. Soil sampler for rocky soils. US Department of Agriculture, Forest Service, North
496 Central Forest Experiment Station.
- 497 Radcliffe, D.E. and Šimůnek, J., 2018. *Soil physics with HYDRUS: Modeling and applications*. CRC press.
- 498 Ravina, I. and Magier, J., 1984. Hydraulic conductivity and water retention of clay soils containing coarse fragments.
499 *Soil Science Society of America Journal*, 48(4), pp.736-740., doi:10.2136/sssaj1984.03615995004800040008x.
- 500 Russo, D., 1988. Determining soil hydraulic properties by parameter estimation: On the selection of a model for the
501 hydraulic properties. *Water resources research*, 24(3), pp.453-459, doi: 10.1029/WR024i003p00453.
- 502 Sarkar, S., Germer, K., Maity, R. and Durner, W., 2019. Measuring near-saturated hydraulic conductivity of soils by
503 quasi unit-gradient percolation—1. Theory and numerical analysis. *Journal of Plant Nutrition and Soil Science*, 182(4),
504 pp.524-534, doi: 10.1002/jpln.201800382.
- 505 Schelle, H., Iden, S.C., Peters, A. and Durner, W., 2010. Analysis of the agreement of soil hydraulic properties
506 obtained from multistep-outflow and evaporation methods. *Vadose Zone Journal*, 9(4), pp.1080-1091, doi:
507 10.2136/vzj2010.0050.
- 508 Schelle, H., Durner, W., Schlüter, H., Vogel, H.-J. and Vanderborght, J., 2013. Virtual Soils: Moisture measurements
509 and their interpretation by inverse modeling, *Vadose Zone Journal* 12:3, doi:10.2136/vzj2012.0168.
- 510 Schindler, U., Durner, W., von Unold, G. and Müller, L., 2010. Evaporation method for measuring unsaturated
511 hydraulic properties of soils: Extending the measurement range. *Soil science society of America journal*, 74(4),
512 pp.1071-1083.
- 513 Schofield, R.K., 1935. The pF of water in soil. In *Trans. of the Third International Congress on Soil Science*, 2, Plenary
514 Session Papers, 30 July-7 August, 1935 Oxford, UK (pp. 37-48).
- 515 Sekucia, F., Dlapa, P., Kollár, J., Cerdá, A., Hrabovský, A. and Svobodová, L., 2020. Land-use impact on porosity
516 and water retention of soils rich in rock fragments. *CATENA*, 195, p.104807.
- 517 Šimůnek, J., Van Genuchten, M.T. and Šejna, M., 2006. The HYDRUS software package for simulating two-and
518 three-dimensional movement of water, heat, and multiple solutes in variably-saturated media. Technical manual,
519 version, 1, p.241.
- 520 Šimůnek, J., van Genuchten, M.T. and Šejna, M., 2008. Development and applications of the HYDRUS and
521 STANMOD software packages and related codes. *Vadose Zone Journal*, 7(2), pp.587-600, doi: 10.2136/vzj2007.0077.
- 522 Šimůnek, J., Van Genuchten, M.T. and Šejna, M., 2016. Recent developments and applications of the HYDRUS
523 computer software packages. *Vadose Zone Journal*, 15(7), doi: 10.2136/vzj2016.04.0033.
- 524 Singh, A., Haghverdi, A., Öztürk, H.S. and Durner, W., 2020. Developing Pseudo Continuous Pedotransfer Functions
525 for International Soils Measured with the Evaporation Method and the HYPROP System: I. The Soil Water Retention
526 Curve. *Water*, 12(12), p.3425.



- 527 Singh, A., Haghverdi, A., Öztürk, H.S. and Durner, W., 2021. Developing Pseudo Continuous Pedotransfer Functions
 528 for International Soils Measured with the Evaporation Method and the HYPROP System: II. The Soil Hydraulic
 529 Conductivity Curve. *Water*, 13(6), p.878.
- 530 Stevenson, M., Kumpan, M., Feichtinger, F., Scheidl, A., Eder, A., Durner W., and Strauss, P., 2021. Innovative
 531 method for installing soil moisture probes in a large-scale undisturbed gravel lysimeter, *Vadose Zone Journal* 2021;
 532 1–7. DOI: 10.1002/vzj2.20106.
- 533 Tetegan, M., de Forges, A.R., Verbeque, B., Nicoulaud, B., Desbourdes, C., Bouthier, A., Arrouays, D. and Cousin,
 534 I., 2015. The effect of soil stoniness on the estimation of water retention properties of soils: A case study from central
 535 France. *Catena*, 129, pp.95-102, doi: 10.1016/j.catena.2015.03.008.
- 536 Van Genuchten, M.T., 1980. A closed-form equation for predicting the hydraulic conductivity of unsaturated soils.
 537 *Soil Sci. Soc. Am. J.* 44:892-898, doi: 10.2136/sssaj1980.03615995004400050002x.
- 538 Verbist, K.M.J., Cornelis, W.M., Torfs, S. and Gabriels, D., 2013. Comparing methods to determine hydraulic
 539 conductivities on stony soils. *Soil Science Society of America Journal*, 77(1), pp.25-42. Wang, W., Sun, L., Wang,
 540 Y., Wang, Y., Yu, P., Xiong, W., Shafeeqe, M. and Luo, Y., 2020. A convex distribution of vegetation along a stony
 541 soil slope due to subsurface flow in the semiarid Loess Plateau, northwest China. *Journal of Hydrology*, 586, p.124861,
 542 doi: 10.1016/j.jhydrol.2020.124861.
- 543 Zhang, Y., Zhang, M., Niu, J., Li, H., Xiao, R., Zheng, H. and Bech, J., 2016. Rock fragments and soil hydrological
 544 processes: significance and progress. *Catena*, 147, pp.153-166, doi: 10.1016/j.catena.2016.07.012.
- 545 Zimmerman, R. W., and Bodvarsson, G.S., 1995. The effect of rock fragments on the hydraulic properties of soils.
 546 Lawrence Berkeley Lab., CA, USA, USDOE, Washington, D.C., USA, doi: 10.2172/102527.